RZ 3481 (# 99376) 09/08/03
Mathematics & Physics 11 pages

Research Report

Nanometer-Scale View of the Electrified Interface: A Scanning Probe Microscopy Study

P. Müller, L. Rossi and S.F. Alvarado
IBM Research
Zurich Research Laboratory
8803 Rüschlikon
Switzerland

LIMITED DISTRIBUTION NOTICE

This report has been submitted for publication outside of IBM and will probably be copyrighted if accepted for publication. It has been issued as a Research Report for early dissemination of its contents. In view of the transfer of copyright to the outside publisher, its distribution outside of IBM prior to publication should be limited to peer communications and specific requests. After outside publication, requests should be filled only by reprints or legally obtained copies of the article (e.g., payment of royalties). Some reports are available at http://domino.watson.ibm.com/library/Cyberdig.nsf/home.

Research
Almaden · Austin · Beijing · Delhi · Haifa · T.J. Watson · Tokyo · Zurich

Nanometer-Scale View of the Electrified Interface: A Scanning Probe Microscopy Study

P. Müller*, L. Rossi, S. F. Alvarado
IBM Research, Zurich Research Laboratory, 8803 Rüschlikon, Switzerland

Narrowing the dimensions of electrified interfacial systems from the microscopic to the nanometer scale leads to unexpected effects. The morphology of nanometer-scale thin films on a defined substrate is an important parameter as it strongly influences the transport properties of charge carriers in thin films. At an organic/metal or an organic/organic interface, the morphological phase and the manner how the molecules interact with the substrate are a determining factor for the energies needed to inject charge carriers into the thin film. Scanning probe microscopy is a powerful method for characterizing surface morphologies with nanometer-scale spatial resolution. Electronic bulk and interfacial properties are detectable when the tip of a scanning tunneling microscope in constant-current mode penetrates an organic thin film (*z*-*V* spectroscopy). In this way, the injection energies for positive charge carriers (holes) into the highest occupied molecular orbitals and of negative charge carriers (electrons) into the lowest unoccupied molecular orbitals can be determined. From *z*-*V* spectroscopy data, it is possible to derive the so-called single particle energy gap (E_{gsp}), which is a measure of the energy gap for bipolar charge injection at the interface. By combining E_{gsp} with the optical adsorption gap (E_a) of the material, the exciton binding energy (E_b) can be determined. The model for an organic/metal interface applied most often assumes the existence of a common vacuum level (CVL). Measurements were carried out on sublimated thin films of monomers on gold substrates. The results reveal differences to the CVL model, which are due to the formation of a dipole layer at the interface. This affects charge-carrier transport and the injection energy, as well as triggers charge injection into optically inactive molecular orbital states, which can result in a smaller E_{gsp} than optical band-gap measurements predict.

1. Introduction

The continuing research interest in shrinking the dimensions of electronic devices from the micrometer to the nanometer scale is of great importance. On the one hand, this trend is driven by economic reasons and on the other hand by current technological needs. Shrinking the dimensions of electrified interfacial systems from the micrometer- to the nanometer-scale regime often leads to the appearance of effects in the electronic properties that are not easily scalable. For example, the morphology of nanometer-scale thin films on a defined substrate is an important parameter as it strongly influences the transport properties of charge carriers in thin films. In addition, at organic/metal or organic/organic interfaces, the morphological structure and the way the interfacing molecules interact chemically are determining factors for the electronic properties, and thus crucial for the characteristic energies needed to inject charge carriers.

As an application [1], organic light-emitting devices (OLEDs) consists of a stack of very precise nanometer-thick organic layers, in which each has a specified function [2]. An additional challenge of nanometer-scale structuring is posed by nanometer-sized transistors [3]. Emerging technologies such as spintronics [4] and quantum molecular electronics [5, 6] are based on nanometer-scale physical phenomena. The interest in organic electronic devices is reflected by numerous experimental and theoretical investigations aimed at elucidating the underlying physical processes [7-13]. Particular attention is paid to charge-carrier injection from a metal electrode into an organic thin film or from one organic thin film into another, and charge-carrier transport within the organic thin films, all of which are crucial parameters for device operation.

Scanning tunneling microscopy (STM) imaging has proved to be a powerful tool to investigate these processes locally with a resolution on the nanometer scale. Moreover, characterization by STM distance versus potential (*z-V*) spectroscopy can be used to determine accurate values for the electronic properties, especially of organic materials. For an overview of STM-based techniques in this field, the reader is referred to [14-16].

The barriers for the injection of charge carriers from a metal electrode into an organic thin film are determined by the work function of the metal electrode, and the energy levels of the highest occupied (HOMO) and the lowest unoccupied molecular orbital (LUMO) of the organic film. Typically, the position of the HOMO level (E_H) with respect to the Fermi level of the metal electrode (E_F) is set equal to the difference in the ionization potentials (IPs) of the materials and the work function of the metal (Φ_w), usually obtained by means of ultraviolet (UPS) or x-ray photon spectroscopy (XPS), or by cyclic voltametry (CV) experiments,

$$E_H = IP_o - \Phi_w \,. \tag{1}$$

This is the so-called common vacuum level (CVL) approximation [17], see Figure 1a. The position of the LUMO level (E_L) relative to E_F is then calculated by adding the optical absorption band gap (E_a) to E_H,

$$E_L = E_H + E_a \,, \tag{2}$$

where E_a is taken from the optical absorption spectrum.

However, Equation (1) neglects the influence of interfacial effects such as dipole layers and image forces, and the calculation of E_L, done using Equation (2), takes neither the exciton binding energy (E_b) [18, 19] nor the exciton dissociation energy [20] into account. In organic materials, E_b is important because it exceeds the thermal energy (kT) at room temperature (RT). The CVL approximation also disregards the molecular levels of optically inaccessible electronic states at the interface. Evidence of significant deviations of the CVL model for the organic-metal interface has been widely reported in studies based on techniques such as UPS and XPS [9, 21-25], internal photoemission [19, 26], and STM [27, 28]. Figure 1b depicts an extended model that takes all the deviations into account.

2. STM *z-V* Spectroscopy

In the following, it is discussed how STM *z-V* spectroscopy can be used as a direct probe of the injection energies, E_{p-} and E_{p+}, for electrons and holes into polaronic states, respectively, of an organic material, see Figure 1b. In contrast to conventional STM current-voltage (*I-V*) spectroscopy [29-31], which has to open the feedback loop during operation and measures the energy dependence of the density of states (DOS) [32], STM *z-V* spectroscopy probes the DOS via the voltage-dependent tip displacement at constant tunneling current. Figure 2 shows the three phases of a *z-V* spectrum of a thin film, labeled A, B and C. An example of a complete *z-V* spectrum is depicted in Figure 3.

Under standard STM conditions, the tunneling resistance (R_t) is much larger than the resistance of the organic layers (R_{org}), and the parasitic resistance through the sample (spreading resistance) can be neglected, see Figure 2, Phase A. Thus R_t in Ω is given by

$$R_t = V_t \,/\, I_t \,, \tag{3}$$

where V_t is the tunneling bias voltage applied and I_t the tunneling current. Charge-carrier injection occurs through the vacuum barrier into the organic material. This means that V_t drops almost completely at the vacuum tunneling barrier. The charge-injection energy, E_t in eV, can be tuned by adjusting the magnitude and polarity of V_t:

$$E_t = V_t\, e\ , \tag{4}$$

where e is the single electron charge. The polarity of V_t determines the type of polarons to inject (electrons or holes). Reducing the bias voltage under constant-current conditions first forces the tip into close proximity of and ultimately into direct physical contact with the organic thin film ($R_{\mathrm{org}} \geq R_t$), causing the vacuum barrier to collapse.

When this contact mode has been attained, the Fermi level of the tip, E_{Ft}, is typically located at an energy level within the forbidden energy gap of the organic material, see Figure 2, Phase B. The high electrical field across the organic layer leads to band bending and to the formation of a Schottky-like diode. The gradient of the electric field strongly depends on the curvature of the injecting electrodes. Thus, the highest electric-field drop appears at the apex of the STM tip, which under ideal conditions will be the predominant site for charge-carrier injection into the organic thin film. For example, with a typical STM tip-apex radius of $R \simeq 50$ nm, one can obtain continuous injection current densities in the range of $j = 10$ to 10^4 A/cm^2 at a V_t of a few volts, which is orders of magnitude higher than current densities for the planar interface between the organic material and the metal electrode. This is in agreement with the qualitative statement that in an organic thin film the electric field gradient as a function of distance is linear for an atomically flat electrode, whereas it is quadratically dependent on the inverse of the radius for an STM tip apex. Consequently, the current passing through the STM-tip–thin-film-substrate system is expected to be dominated by a unipolar injection of charge carriers from the STM tip. Note that step sites of rough substrates may act as injection points, which can lead to bipolar charge-carrier injection. The injection process can either be thermionic emission or tunneling [33, 34], depending on the barrier heights, the field strength at the interface, and temperature. For barrier heights of approximately 1 eV and average fields in the range of 0.1 to 1 V/nm, mainly tunneling injection [35] has to be expected, whereas at barrier heights well below 1 eV thermionic emission might become significant. A more detailed description of tip geometries and their local current densities can be found in [14, 36, 37]. Regarding tip penetration, if the magnitude of V_t is decreased for constant I_t, the STM feedback loop causes a decrease of the tip-sample distance d to compensate the decrease in R_t. In other words, the tip motion compensates the reduction of the electric field associated with the change in V_t to maintain a constant tunneling current across the barrier. Because the tip contact area increases with decreasing d, the electric field required for injection and transport should be reduced when the tip moves into the sample. This effect, however, is relatively small owing to the exponential dependence of the injection probability on the electric field and the geometrical dependencies of the tip discussed. Therefore, the effective injection area can be treated as constant throughout Phase B, except at the very early stage, when the vacuum barrier collapses and the tip enters into contact with the thin film.

Injection of charge carriers into the organic material is possible until $|V_t|$ has been reduced to the value at which the Fermi level of the tip enters the forbidden energy gap at the interface with the metal electrode, see Figure 2, Phase C. The point at which this transition occurs determines the position of the lowest electron polaron state (E_{p-}) for an applied $V_t < 0$ V or of the highest polaron state (E_{p+}) for $V_t > 0$ V. In this phase, a characteristic logarithmic z-V curve is observed when either tunneling directly into the metal electrode or nonresonantly through a monomolecular organic layer in contact with the electrode. The transition between Phases B and C, which is typically marked by a sharp decrease in the steepness of the z-V curve, is a direct measure of the potential barrier to inject either electrons or holes from a buried electrode into a thin film.

Note that the z-V technique works only for fluids and soft materials that yield to the pressure exerted by the STM tip.

From the polaronic quantities E_{p-} and E_{p+} measured, the single-particle energy gap (E_{gsp} in eV) can be obtained by taking [19]

$$E_{gsp} = E_{p-} - E_{p+} \, . \tag{5}$$

The combination of an electron polaron (p–) and a hole polaron (p+) results in the formation of an exciton. The exciton binding energy (in eV) has been defined [18] as

$$E_b = E_{gsp} - E_a \, , \tag{6}$$

where E_a is the energy required to create a molecular excitation as determined from optical absorption spectra. Equations (5) and (6) show that supplying the exciton with the energy E_b creates a pair of oppositely charged polarons. In an organic material, for example, the radiative decay of such a singlet exciton results in the emission of a photon.

The local mobilities of the electrons (μ^-) and holes (μ^+) of relevance in charge-carrier transport can be qualitatively estimated by comparing the slopes (dz/dV) of the z-V curves for Phase B in Figure 2. For a given I_t and a thin film of thickness D, one can see that, to sustain the current flow through the injection area, a lower electric field is required for a high-conductance than for a low-conductance material. Thus, in contact mode (Phase B), the average slopes of the z-V curves are directly affected by the local conductivity of the sample. This implies that in point-contact mode, z-V curves contain information about the transport properties of organic materials. Experiments indicate that for a given sample conductance the rate of the tip penetration is proportional to R_t, (see short-dashed line in Figure 3).

3. Experimental Details

The measurements were carried out at RT under ultrahigh vacuum (UHV) conditions, typically at a base pressure in the 10^{-10} mbar range. An adjacent treatment chamber is equipped with the instrumentation used for substrate cleaning and preparation. The detailed description of the experimental setup can be found in [15, 38]. To acquire the STM z-V spectra, commercial ion-milled platinum-iridium tips were used. The organic thin films of tris-(8-hydroxyquinoline)aluminum (Alq_3) and copper phthalocyanine (CuPc) were prepared *in situ* by thermal evaporation on atomically flat Au(111) and Ag(111) single-crystal substrates at RT [14]. The as-grown organic thin films are typically 3 to 5 nm thick. For further details regarding sample preparation and the morphologies observed using STM, the reader is referred to [14, 27, 39].

3.1 Alq_3 Thin Films on Au(111)

STM images taken at different locations and on various samples reveal that the surface of very thin (a few nanometer thick) films exhibits unaligned nano-crystallites [14]. Figure 3 shows a typical z–V spectroscopy curve collected on Alq_3 on Au(111). For this system we statistically obtained $E_{p-} = 1.15 \pm 0.18$ eV for electron injection and $E_{p+} = -1.81 \pm 0.25$ eV for hole injection, relative to the Au(111) Fermi level.

In comparing the barrier-height values determined by z-V spectroscopy with those predicted by the CVL approximation, bearing in mind the measurement uncertainties, only differences of more than 0.3 to 0.4 eV are significant. The scatter of IP values reported in the literature is in this range. Despite this deviation, the CVL model predicts higher energy levels for Alq_3 on a Au(111) substrate than the result obtained by z-V spectroscopy. Using Equations (1) and (2), the barrier height for electron injection (see Figure 1a) can be estimated to be $E_L = 1.9$ to 2.5 eV, for

$\Phi_{Au(111)}$ = 5.31 eV [26], the IP_{Alq3} = 5.57 to 6.0 eV [21, 22, 40-42], and the optical band gap measured on an Alq_3 thin film E_a = 2.5 eV [43]. The direct measurement by *z-V* spectroscopy (Figure 1b), however, yields E_{p-} = 1.15 eV. The single-particle energy gap obtained from Equation (5) is E_{gsp} = 2.96±0.13 eV, which is clearly higher than E_a derived from the optical-absorption band gap [44]. Using Equation (6), an exciton binding energy as high as 0.46±0.13 eV can be obtained.

It is also found that for an Alq_3 thin film the electron injection barrier is approximately 0.2 eV higher on Au(111) than on Ag(111) [14]. The magnitude of this shift is much smaller than the value of 0.57 eV calculated in the framework of the CVL model by taking the difference between the work functions of the two surfaces ($\Phi_{Ag(111)}$ = 4.74 eV [45]).

All these deviations from the pure CVL model indicate the effect of image forces or the formation of a dipole layer at the interface owing to the transfer of negative charges from Alq_3 to the metal substrate. The value for E_{p+} confirms the results of UPS measurements on the Alq_3/Au(111) interface [9, 21, 22].

A statistical analysis of measurements taken on Au(111) and Ag(111) yields a distribution of injection thresholds for electrons that exhibits a peak at $E_{p-} \simeq 1.15$ and $\simeq 1.7$ eV, respectively. This indicates that two different types of surface configurations exist between the organic material and the metal electrode. The E_{gsp} values for the two configurations are 2.96 and 3.04 eV. This behavior can either be explained by the different morphologies of the Alq_3 thin films [46], the different electronic properties of the two existing Alq_3 isomers, the meridianal and the facial configurations [47], or by different orientations of the Alq_3 on the substrate [14, 27, 48].

The slope dz/dV of the *z-V* curve of Phase B acquired with negative tip bias (E_{p-}) is much steeper than that of the curve taken with positive tip bias (E_{p+}). As discussed in [14], this confirms that Alq_3 preferentially transports electrons and that μ^- is much higher than μ^+ [49].

3.2. CuPc Thin Films on Au(111)

STM images of CuPc thin films grown on a Au(111) substrate at RT are featureless, indicating that these films are completely disordered. After annealing at 600 K for 1 h, however, the organic thin film was found to crystallize, exhibiting various polymorphic phases (see Figure 4). The crystallites are about 30 to 40 monomolecular layers thick, several 100 nm in diameter, and strongly resemble the bulk α and β phases [39]. Three examples are shown in Figure 5.

On the disordered phase, the injection energies measured for electrons and holes are E_{p-} = 0.55±0.15 and E_{p+} = –0.55±15 eV, respectively, relative to the E_F of the Au(111) metal electrode, yielding E_{gsp} = 1.1±0.2 eV [39]. In a statistical analysis of the polymorph phases α, β_1 and β_2 (see Figure 5), the following injection energies were measured: E_{p-} = 0.08±0.04, 0.21±0.07, and 0.1±0.05 eV, and E_{p+} = –0.1±0.04, –0.62±0.17, and –0.2±0.05 eV, relatively to the E_F of the Au(111) substrate. The results suggest very small single-particle energy gaps of E_{gsp} = 0.18±0.06, 0.83±0.19, and 0.3±0.07 eV, respectively.

Considering the ionization potentials reported for CuPc thin films, IP_{CuPc} = 4.7 to 5.3 eV [40, 42, 50, 51], an E_H = 0 to 0.6 eV relative to the E_F of the Au(111) substrate would be expected when applying the CVL approximation. Theoretically, both the HOMO and the LUMO level are equal to or higher than the E_F of the Au(111) substrate. The results show, however, that in all cases E_H is negative; therefore, the HOMO level clearly lies below the Fermi level of the Au(111) substrate, which indicates the presence of a dipole layer, of a net charge at the interface, or the effect of image forces.

The slopes of the *z-V* curves acquired on polymorphic thin films are approximately one order of magnitude steeper than that of the disordered phase, indicating much higher μ^- and μ^+ values for polycrystalline molecular arrangements [39].

In general, the polymorphic phases of CuPc thin films seem to exhibit a much smaller E_{gsp} than the disordered samples do [39]. This clearly reflects the influence of the molecular packing on the energy levels. In both cases, i.e. in disordered and polymorphic films, E_{gsp} appears to be smaller than the optical-absorption band gap E_a = 1.6 to 1.7 eV, as reported in the literature [52, 53]. This suggests that charge carriers are injected from the Au(111) substrate into optically inactive states of the CuPc thin film. Note, however, that this interpretation assumes unipolar injection from the tip. For a detailed theoretical discussion of the effect of optically inactive states, the reader is referred to [16, 39].

4. Concluding Remarks

Scanning probe microscopy is a powerful tool for characterizing surface morphologies with nanometer-scale spatial resolution. Applying *z-V* spectroscopy, the electronic bulk and interfacial properties of organic/substrate and organic/organic as well as of solution/substrate interfaces can be analyzed. An important capability of this technique is that it allows the direct measurement of the molecular-level alignments of both occupied and empty states. In addition, it is also possible to probe charge-carrier injection into electronic states that optically are inaccessible.

From the injection barriers (E_{p-} and E_{p+}), the single-particle energy gap (E_{gsp}) and, together with the optical-absorption band gap (E_a), the exciton binding energy (E_b) can be calculated. Furthermore, a qualitative measure of the local electron and hole mobilities can be derived from the slope dz/dV of the *z-V* curves.

Measurements at the Alq_3 / Au(111) interface reveal that, because of the formation of a dipole layer or effects of image forces, a potential shift is induced that influences the injection energy for charge carriers. The CuPc/Au(111) system turned out to be an ideal case for investigating the influence of the morphology, which can be disordered or polymorph. Charge-carrier transport clearly increases with the molecular-packaging density, whereas E_{gsp} is reduced. In all measurements on the CuPc/Au(111) system, a smaller energy for the single-particle gap than for the optical-absorption band gap was observed. That indicates charge injection into optically inaccessible polaronic states.

Because the injection barriers for electron- and hole-charge carriers obtained from STM *z–V* spectroscopy are quantitatively very accurate, they form an ideal basis for future theoretical investigations and interface modeling.

As mentioned above, measuring electronic properties by means of STM *z-V* spectroscopy is applied to thin films consisting of soft materials or to solution-based systems. Investigations of more rigid material systems, however, would be of great interest, in particular in the field of semiconductors.

5. Acknowledgments

Some of this work was performed within the Training and Mobility of Researchers Network EUROLED, and supported by grants from the Swiss Federal Office for Education and Science and by the European Commission. The authors thank W. Riess for his support and fruitful discussions as well as the IBM Zurich Lab's Engineering and Publications groups for their help.

6. References

[1] T. Tsujimura, Y. Kobayashi, K. Murayama, A. Tanaka, M. Morooka, E. Fukumoto, H. Fujimoto, J. Sekine, K. Kanoh, K. Takeda, K. Miwa, M. Asano, N. Ikeda, S. Kohara, S. Ono, C.-T. Chung, R.-M. Chen, J.-W. Chung, C.-W. Huang, H.-R. Guo, C.-C. Yang, C.-C. Hsu, H.-J. Huang, W. Rieß, H. Riel, S. Karg, T. Beierlein, D. Gundlach, S. F. Alvarado, C. Rost, P. Müller, F. Libsch, M. Maestro, R. Polastre, A. Lien, J. Sanford, R. Kaufmann, in: *Society for Information Display Symposium (SID 03), Baltimore, MD. Technical Digest*, **2003**, Paper 4.1, p. 6.

[2] W. Rieß, H. Riel, T. Beierlein, W. Brütting, P. Müller, P. F. Seidler, *IBM J. Res. Develop*. **2001**, *45*, 770.

[3] B. Doris, M. Ieong, T. Kanarsky, Y. Zhang, R. A. Roy, O. Dokumaci, Z. Ren, F.-F. Jamin, L. Shi, W. Natzle, H.-J. Huang, J. Mezzapelle, A. Mocuta, S. Womack, M. Gibelyuk, E. C. Jones, R. J. Miller, H. S. Philip, W. Haensch, in: *IEEE International Electron Devices Meeting (IEDM 02), San Francisco, CA*, *Technical Digest*, **2002**, Paper 10.6.1, p. 267.

[4] S. Das Sarmas, *Am. Sci*. **2001**, *89*, 516.

[5] R. Martel, T. Schmidt, H. R. Shea, T. Hertel, Ph. Avouris, *Appl. Phys. Lett.* **1998**, *73*, 2447.

[6] L. M. K. Vandersypen, M. Steffen, G. Breyta, C. S. Yannoni, R. Cleve, I. L. Chuang, *Phys. Rev. Lett*. **2000**, *85*, 5452.

[7] H. Ishii, K. Sugiyama, E. Ito, K. Seki, *Adv. Mater*. **1999**, *11*, 605.

[8] A. Rajagopal, C. I. Wu, A. Kahn, *J. Appl. Phys*. **1998**, *83*, 2649.

[9] S.T. Lee, X. Y. Hou, M. G. Mason, C. W. Tang, *Appl. Phys. Lett*. **1998**, *72*, 1593.

[10] W. Brütting, S. Berleb, A. Mückel, *Org. Electron*. **2001**, *2*, 1.

[11] H. Bässler, *phys. status solidi b* **1993**, **175**, 15.

[12] N. Graham, R. Friend, in: *Solid State Physics, Advances in Research and Applications* (Eds: H. Ehrenreich, F. Spaepen), Academic Press, San Diego, CA, **1995**, Vol. 49, p. 2.

[13] L. Yan, Y. Gao, *Thin Solid Films* **2002**, *417*, 101.

[14] S. F. Alvarado, L. Rossi, P. Müller, P. F. Seidler, *IBM J. Res. Develop*. **2001**, *45*, 89.

[15] P. Müller, S. F. Alvarado, L. Rossi, W. Rieß, *Mater. Phys. Mech*. **2001**, *4*, 76.

[16] S. F. Alvarado, in *Conjugated Polymer and Molecular Interfaces* (Eds.: W. R. Salaneck, K. Seki, A. Kahn, J.-J. Piraux), Marcel Dekker Inc., New York, **2001**, p 473.

[17] W. Schottky, *Z. Phys*. **1942**, *118*, 539.

[18] E. M. Conwell, *Synth. Met*. **1996**, *83*, 101.

[19] I. H. Campbell, T. W. Hagler, D. L. Smith, J. P. Ferraris, *Phys. Rev. Lett.* **1996**, *76*, 1900.

[20] D. Woehrle, L. Kreienhoop, D. Schlettwein, in: *Phthalocyanines Properties and Applications* (Eds.: C. C. Leznoff, A. B. P. Lever), VCH Publishers, New York, **1996**, Vol. 4, p. 223.

[21] K. Sugiyama, D. Yoshimura, T. Miyamae, T. Miyazaki, H. Ishii, Y. Ouchi, K. Seki, *J. Appl. Phys*. **1998**, *83*, 4928.

[22] A. Rajagopal, C. I. Wu, A. Kahn, *J. Appl. Phys*. **1998**, *83*, 2649.

[23] T. Mori, H. Fujikawa, S. Tokito, Y. Taga, *Appl. Phys. Lett*. **1998**, *73*, 2763.

[24] R. Schlaf, B. A. Parkinson, P. A. Lee, K. W. Nebesny, A. R. Armstrong, *J. Phys. Chem. B* **1999**, *103*, 2984.

[25] S. C. Veenstra, U. Stalmach, V. V. Krasnikov, G. Hadziioannou, H. T. Jonkman, A. Heres, G. Sawatsky, *Appl. Phys. Lett*. **2000**, *76*, 2253.

[26] G. L. J. Rikken, Y. A. R. R. Kessener, D. Braun, E. G. J. Staring, A. Demandt, *Synth. Met*. **1994**, *67*, 115.

[27] S. F. Alvarado, L. Libioulle, P. F. Seidler, *Synth. Met*. **1997**, *91*, 69.

[28] S. F. Alvarado, P. F. Seidler, D. G. Lidzey, D. D. C. Bradley, *Phys. Rev. Lett*. **1998**, *81*, 1082.

[29] N. D. Lang, *Phys. Rev. Lett.* **1987**, *58*, 45.

[30] S. De Cheveigne, J. Klein, A. Leger, in: *Tunneling Spectroscopy* (Ed. P. K. Hansma), Plenum Press, New York, **1982**, p. 109.

[31] R. Wiesendanger, *Scanning Probe Microscopy and Spectroscopy, Methods and Applications*, Cambridge University Press, Cambridge, UK, **1994**.

[32] R. Feenstra, *Phys. Rev. B* **1994**, *50*, 4561.

[33] E. M. Conwell, E. W. Wu, *Appl. Phys. Lett*. **1997**, *70*, 1867.

[34] M. N. Bussac, D. Michoud, L. Zuppiroli, *Phys. Rev. Lett.* **1998**, *81*, 1678.

[35] A. van der Ziel, in: *Solid State Physical Electronics*, Third Edition (Ed.: N. Holonyak), Prentice-Hall, Inc., Englewood Cliffs, NJ, **1976**, pp. 152-183.

[36] M. A. Lampert, P. Mark, *Current Injection in Solids* (Eds. H. G. Booker, N. DeClaris), Academic Press, New York, **1970**.
[37] M. K. Miller, A. Cerezo, M. G. Hetherington, G. D. W. Smith, in: *Atom Probe Field Ion Microscopy*, Oxford University Press, Oxford, UK, **1996**, p. 41.
[38] S. F. Alvarado, W. Rieß, M. Jandke, P. Strohriegl, *Org. Electron*. **2001**, *2*, 75.
[39] S. F. Alvarado, L. Rossi, P. Müller, W. Rieß, *Synth. Met*. **2001**, *122*, 73.
[40] C. Hosokawa, H. Higashi, H. Nakamura, T. Kusumoto, *Appl. Phys. Lett*. **1995**, *67*, 3853.
[41] M. Propst, R. Haight, *Appl. Phys. Lett*. **1997**, *71*, 202.
[42] S. T. Lee, Y. M. Wang, X. Y. Hou, C. W. Wang, *Appl. Phys. Lett*. **1999**, *74*, 670.
[43] A. Aziz, K. L. Narasimhan, *Synth. Met*. **2002**, *131*, 71.
[44] S. F. Alvarado, W. Rieß, *Materials Research Society Proc.* **2001**, *665*, 121.
[45] H. B. Michaelson, *J. Appl. Phys*. **1977**, *48*, 4729.
[46] M. Birkmann, G. Gadret, M. Muccini, C. Taliani, N. Masciocchi, A. Sironi, *J. Am. Chem. Soc*. **2000**, *122*, 5147.
[47] M. Amati, F. Leji, *J. Phys. Chem. A* **2003**, *107*, 2560.
[48] A. Curioni, W. Andreoni, *IBM J. Res. Develop*. **2001**, *45*, 101.
[49] T. Tsutsui, H. Tokuhisa, M. Era, in: *Polymer Photonic Devices* (Eds.: B. Kippelen, D. D. C. Bradley), *Proc. SPIE*, SPIE, Bellingham, WA, **1998**, Vol. 3281, p. 230.
[50] T. Chassé, C.-I. Wu, I. G. Hill, A. Kahn, *J. Appl. Phys*. **1999**, *85*, 6589.
[51] A. J. Ikushima, T. Kanno, S. Yoshida, A. Maeda, *Thin Solid Films* **1996**, *273*, 35.
[52] E. A. Lucia, F. D. Verderame, *J. Chem. Phys*. **1968**, *48*, 2674.
[53] B. R. Hollebone, M. J. Stillman, *J. Chem. Soc. Faraday Trans. II* **1978**, *74*, 2107.

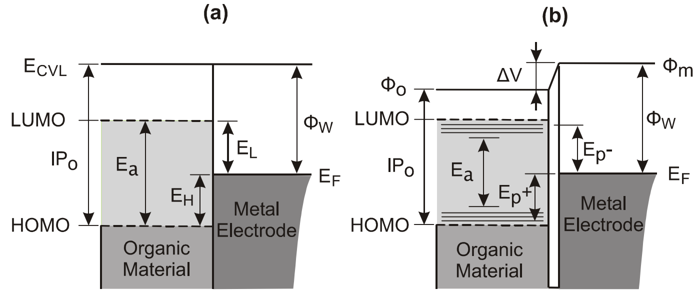

Figure 1. (a) Schematic of the common vacuum level (CVL) model, where E_{CVL} is the absolute vacuum level, Φ_W the work function of the electrode, E_F the Fermi level of the electrode, LUMO the level of the lowest unoccupied and HOMO the level of the highest occupied molecular orbital, E_L (E_H) the injection energy for electrons (holes) relative to E_F, IP_O the ionization potential of the organic thin film, and E_a the optical-absorption band gap. (b) Schematic of the extended CVL model. A potential shift ΔV is introduced, where Φ_m and Φ_O are the vacuum levels of the electrode and the organic thin film, respectively. This allows the inclusion of the effects of image forces or interfacial dipole layers in the model. The lines below the LUMO and above the HOMO symbolize the polaronic states of the organic thin film, where E_{p-} and E_{p+} are the energies, relative to E_F of the metal electrode, needed to inject charge carriers into these polaronic states. Because of the exciton binding energy and interfacial effects, such as the injection of charge carriers into optically inaccessible states, the optically measured E_a may differ from the HOMO–LUMO gap.

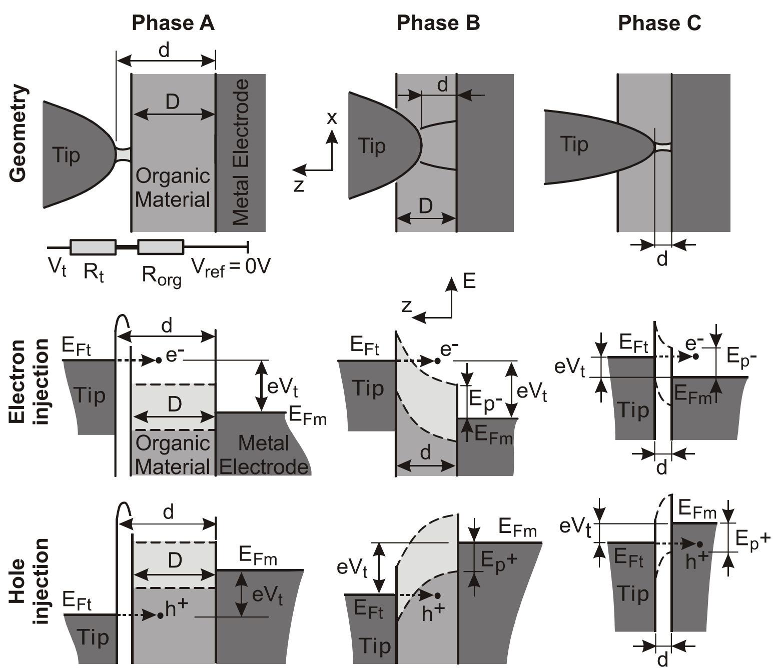

Figure 2. The three phases of a *z-V* spectroscopy measurement. In Phase A, the tip is tunneling in standard STM mode on the organic thin film through a vacuum barrier. The resistor chain shown below the geometrical configuration depicts the relevant resistances between tip and electrode that have to be taken into account. In Phase B, the STM tip first enters into contact with and then penetrates the organic thin film. In Phase C, the tip reaches the electrode and, in the case of a metal, enters the well-known logarithmic *z-V* curve for metals. *D* denotes the thickness of the organic thin film, *d* the tip-to-electrode distance, eV_t the tip potential, e^- and h^+ denote the electron and hole, E_{Fm} and E_{Ft} the Fermi level of the electrode and tip, E_{p-} and E_{p+} the polaronic injection energies for electrons and holes relative to E_{Fm}, *z* and *x* are geometrical dimensions describing the tip movement, and *E* is the electric field.

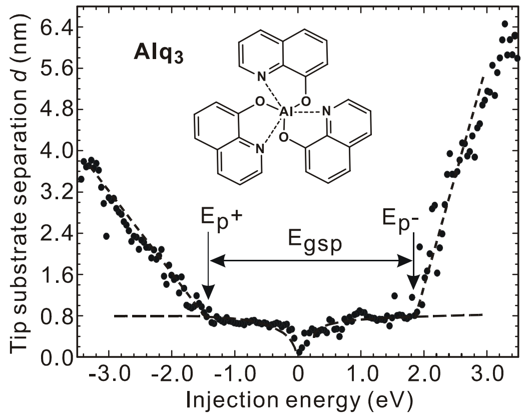

Figure 3. *z-V* spectroscopy curve of Alq_3 on an atomically flat Au(111) single-crystal electrode. The three phases of a *z-V* spectroscopy measurement are clearly visible for electron injection (right-hand side). At energies higher than 3.0 eV, tunneling through a vacuum barrier is observed. Between 3.0 and 1.8 eV, the tip penetrates the Alq_3 thin film. At the point labeled E_{p-}, the tip reaches the DOS of the gold substrate and starts to follow a logarithmic curve that is characteristic of a *z-V* spectrum of a metal (long-dashed line). The same procedure can be applied for the left-hand side, which shows the characteristics for the injection of holes. Note that as a direct consequence of Equation (4), the injection energies for electrons are positive (V_t < 0 V), whereas those for holes are negative (V_t > 0 V). Adapted from [14].

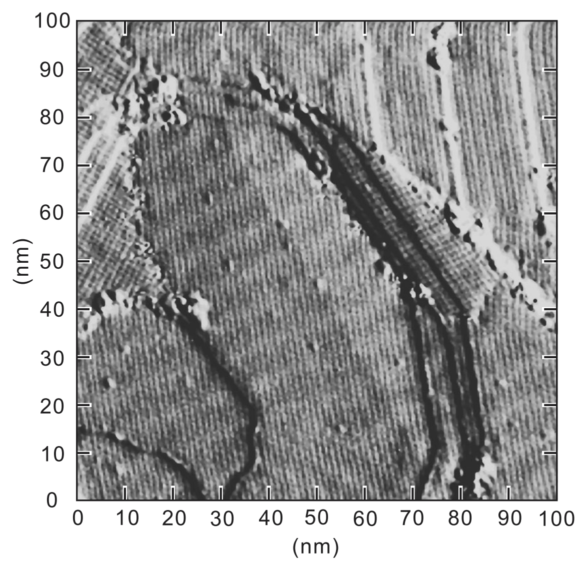

Figure 4. STM image of polymorph grains of CuPc on a Au(111) substrate annealed at 600 K for 1 h. The STM settings were I_t = 1.8 pA and V_t = 3.3 V.

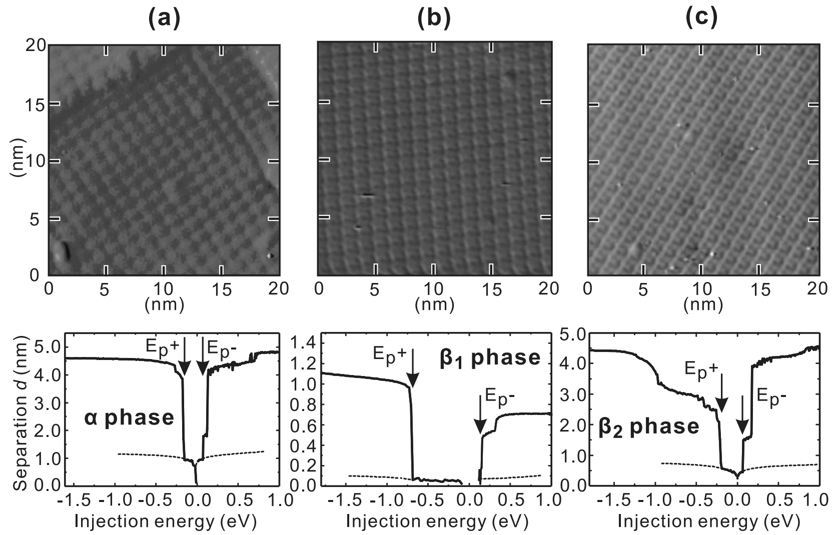

Figure 5. Three morphological phases of CuPc grains grown on Au(111) and their *z*-*V* spectra. The exact values of E_{p-} and E_{p+} have to be obtained by statistical analysis. Panel (a) shows the α-phase (quasi-tetragonal), (b) the β_1 phase (monoclinic), and (c) the β_2 phase (monoclinic). The STM settings were (a) I_t = 20 pA, V_t = 3.5 V; (c) I_t = 60 pA, V_t = –1 V, and (c) I_t = 3 pA, V_t = –1 V. Part (b) adapted from [39].